# From rheological to original three-dimensional mechanical modelling of semi-crystalline polymers: Application to a wide strain rate range and large deformation of Ultra-High Molecular Weight PolyEthylene

C. A. Bernard, O. Lame, T. Deplancke, J-y Cavaillé, Kazuhiro Ogawa

# From rheological to original three-dimensional mechanical modelling of semi-crystalline polymers: application to a wide strain rate range and large deformation of Ultra-High Molecular Weight PolyEthylene

C.A. Bernard[1,2,3,*], O. Lame[4], T. Deplancke[4,†], J.-Y. Cavaillé[3], K. Ogawa[2,3]

[1]Frontier Research Institute for Interdisciplinary Sciences, Tohoku University, Sendai, Japan
[2]Fracture and Reliability Research Institute, Tohoku University, Sendai, Japan
[3]ELyTMaX UMI3757, CNRS–Université de Lyon–Tohoku University, International Joint Unit, Tohoku University, Sendai, Japan
[4]Materials Engineering and Science (MATEIS), CNRS, INSA-Lyon, UMR5510, Université de Lyon, Villeurbanne, France

*Corresponding author: chrystelle.bernard@rift.mech.tohoku.ac.jp

**Abstract**

Ultra-High Molecular Weight semi-crystalline polymers, such as Ultra-High Molecular Weight PolyEthylene (UHMWPE) exhibit strong wear and impact resistance, making them good candidates for structural applications in many industrial fields. At high strain rate and large strain, mechanisms of deformation are quite different from those involved in classical semi-crystalline polymers, mainly because chain disentanglements are almost impossible for very long macromolecules even at temperature far above the melting point. Thus, there is a need to develop specific models for these materials and, from the works of Deplancke and her co-workers (Deplancke et al., 2019; Deplancke et al., 2015) who developed a scalar description based on polymer physics, three-dimensional constitutive equations are developed in this work. The developed model proposes an innovative way to take into account the repartition of strain for a semi-crystalline polymer and more generally for a two-phase material. Moreover, by modelling the evolution of microstructure during the plastic deformation of the material, the model is able to reproduce quite fairly the mechanical behavior of UHMWPE for both loading and unloading.

**Keywords**

UHMWPE, 3D modelling, strain rate dependence, compressive behavior, mechanical coupling

## 1. Introduction

Polymers are world-widely used materials which exhibit interesting properties but complex deformation mechanisms. Even though, during the last decades, the knowledge on the deformation mechanisms has been strongly improved, the transcription of these mechanisms into three-dimensional mechanical models still remains a challenge especially for high molecular weight semi-crystalline polymers. There is thus a need for more precise 3D constitutive equations, as input of Finite Element calculations, for the optimization of structure design. In addition, this is the only way to

[†]Present address: Unité Matériaux et Transformations, CNRS UMR 8207 – Université de Lille, Lille, France

optimize the safety coefficients used to avoid breakage of structures in use: they should account for the risks induced by processing defects, and not for the lack of knowledge of the material itself.

As semi-crystalline polymers are the result of the partial crystallization of amorphous macromolecular arrangements formed during cooling from the liquid state, for high enough molecular weight, a given macromolecule belong to both ordered domains (crystals) and amorphous phase [1]. Segments of chain at the interface between crystal and amorphous domains are so called tie molecules or amorphous confined phase: they insure the local stress transfer from one phase to the other one during macroscopic loading (it is noteworthy that, below melting temperature, crystals play the role of crosslinking nodes of the amorphous chains) [2,3]. Though the typical crystal shape and size of a semi-crystalline polymers depend a lot of its thermal history (cooling rate, heat treatments, etc.), for classical linear polyethylene (high density polyethylene, HDPE), as well as for Ultra-High Molecular Weight Polyethylene (UHMWPE), it consists in lamellae with a thickness of about 10 nm and lateral size up to one micron. At the scale of few tens of nm, crystals and amorphous domains appear as regular stacking of both crystals and amorphous layers having a thickness mainly driven by the crystallinity ratio. At larger scale, as the crystallization starts from nuclei, lamellae are often arranged in more or less spherical spherulites, with radius around 1 to 100 μm. Roughly speaking, a crystallinity ratio of 50% leads to same thickness for both crystalline and amorphous lamellae. Thus, at a larger deformation, crystals appear to play the role of crosslinking nodes, most of the macromolecules being caught by the crystals in a more or less regular 3D arrangement. Because of their very high molecular weight, the macromolecules present curvilinear length in the order of 100 microns for molecular weight of $10^7$ g.mol$^{-1}$, with a gyration radius of about 100 nm. Thus, each macromolecule might link a lot of crystals, but are also entangled many times. As discussed elsewhere [4], the time for disentanglement is so long at temperature below the degradation temperature, that even well above the melting point, such a polymer remains in its rubbery state. Therefore, even if some macromolecules can escape from the crystal during deformation, they form a macromolecular network having the properties of a very soft rubber which properties can be modeled by the rubber elasticity theories.

From a mechanical point of view, the deformation behavior of UHMWPE can schematically be divided into different steps as represented in Figure 1 [3–7]. At small deformation, corresponding to stage I in Figure 1, linear mechanical behavior is observed. It corresponds to the elongation of the confined amorphous phase, partially in parallel with the crystalline phase as discussed below. The second stage (stage II in Figure 1) corresponds to the fragmentation of the crystalline lamellae at the spherulite poles [4,8] leading to a non-linear behavior of the material. In this stage, the yield point appears when the fragmentation of the crystalline lamellae reaches the equatorial regions of the spherulites leading to largely spread crystalline block structures linked together by the confined amorphous phase. At the

beginning of this stage, the stress contribution related to the crystalline lamellae is no more effective; however, the crystal network stress continues to increase thanks to the contribution of the amorphous confined phase [9]. During the third stage (stage III in Figure 1), the crystalline lamellae blocks rotate to align in the stretching direction [8]. Starting from the pole and propagating to the equatorial regions, crystalline blocks undergo fibrillation process which consists in pulling out chains from the crystalline lamellae [4]. Therefore, the folded chains, previously part of the crystalline lamellae, become amorphous increasing the length of the confined amorphous phase. Because of the fibrillation process, the crystalline ratio should decrease. However, induced by the strong orientation of the chains within the fibrils in the loading direction, the formation of new crystalline domains occurs within the fibrils. Because of the successive fibrillation-recrystallization steps, the chain disentanglement is delayed. Finally, when fibrils reach their maximum elongation which corresponds to the last stage (stage IV in Figure 1), locking phenomena occurs and greatly increase stress [8]. Because of the combination of the fibrillation process (during stage III) and the recrystallization process (during stages III and IV), the crystalline ratio appears to keep about constant during all the deformation [10]. However, even though the crystalline ratio does not significantly evolve, the role and size of crystalline domains change drastically during the whole deformation process. This phenomenon needs to be considered in the modeling of the mechanical behavior of such polymers.

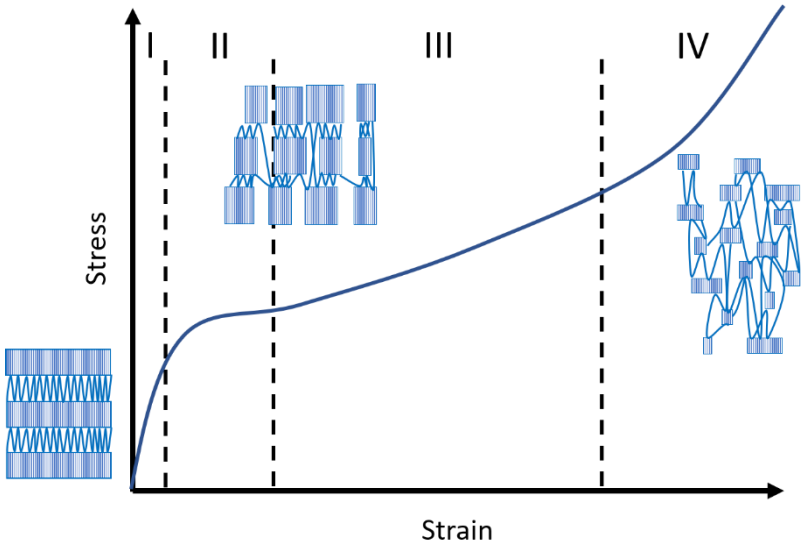


*Figure 1: Schematic representation of the evolution of UHMWPE microstructure in function of its mechanical behavior.*

With the aim of understanding the deformation mechanisms of polymers (amorphous and semi-crystalline polymers), numerous theoretical and numerical models have been developed over the past decades, in addition to the experimental investigations. Numerical models can be divided into two categories: phenomenological models and physical-chemical based models. These latter take into account the molecular relaxations and activated processes at the origin of the deformation mechanisms of the polymer. For this purpose, different theories have been developed to represent

experimental observations. Based on polymer physics, these theories allow modelling the strain rate and temperature sensitivities of the elastic modulus [11–13], the yield stress [14–19] and the orientational hardening [20–24] as well as other phenomena such as cavitation [25,26] and recrystallization [27,28].

Although larger number of theories and numerical models focused on the simulation of amorphous polymers[29–35], several numerical models aim to simulate semi-crystalline polymer behavior. Most of the theories considered the presence of N crystalline inclusions in an amorphous matrix, like Mori-Tanaka model [36,37], self-consistent model [38], three-phase model which considers interface regions between the amorphous matrix and the crystalline inclusions [39,40]. Based on these theories, three-dimensional constitutive models have been developed for semi-crystalline polymers [41–49].

These models usually include generally two branches, composed with a combination of spring and dashpot, acting in parallel as illustrated by Figure 2 [50,51]. The first one, called intermolecular resistance, represents the intermolecular interactions within the crystalline structure (between crystalline lamellae and confined amorphous phase) at the origin of the material's initial stiffness. It usually exists three ways to describe the interactions between crystalline lamellae and confined amorphous phase. Thus it is classical to consider (i) lower bound model (crystalline lamellae and amorphous phase act in series), (ii) upper bound model (crystalline lamellae and amorphous phase act in parallel) [28] and (iii) composite models which consist in an aggregate of layered of two or three-phase composite inclusions [40,52]. In this latter case, these phases are, namely, crystalline lamellae, tie molecules and interphase. The second branch represents the resistance of the macromolecular network to stretching and orientation of the amorphous polymer chain segments. To describe the mechanical behavior of semi-crystalline polymer, simultaneous actions of these branches are necessary. However, while the important stiffness of the first branch comes from the crystalline lamellae and is much more effective at small deformation, the stiffening induced by the second branch comes from the highly reticulated macromolecular network and become predominant at large deformation [48].

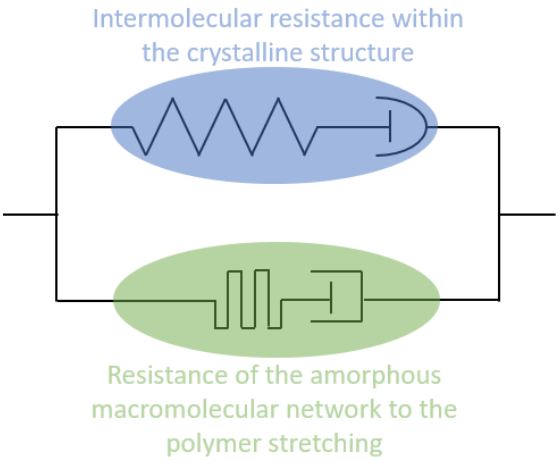


*Figure 2: Schematically representation of the rheological model commonly used for the modelling of semi-crystalline polymers.*

Several researches were focused to model the intermolecular resistance within the crystalline structure (crystalline lamellae and confined amorphous phase). As the deformation of the amorphous confined phase directly influence the deformation of the crystalline phase, it is primordial to that the numerical models takes into account the influence of one phase on the other [8,9,25,46]. An interesting work on the modelling of Ultra High Molecular Weight PolyEthylene was performed by Bergström and Bischoff [53]. The developed Three Network Model, considering three networks acting in parallel, is able to predict the polymer behavior at large strain while taking into account for an evolution of the shear modulus of amorphous phase with respect of the plastic deformation of the crystalline phase. However, it does not consider any microstructural change in the polymer structure (evolution of the crystalline lamellae and confined amorphous phase into fibrils). Thus, to be able to represent the coupling between the crystalline lamellae and confined amorphous phase, combination of parallel and series models was developed. In the idea to improve the current model with the introduction of a physical meaning into the constitutive equations, a recent work of Humbert et al. [54] proposes a model able to capture the coupling between crystalline lamellae and confined amorphous phase. It assumes that crystalline lamellae and confined amorphous phase do not have neither the same kinetics of deformation, nor the same behavior. Thus, from the beginning of the deformation process these two phases are neither in parallel nor in series. At small strain, it is assumed that the stress in the crystalline lamellae is more important than in the confined amorphous phase, whereas, the confined amorphous phase reaches a higher deformation than the crystalline lamellae. During the plastic deformation of the polymer, the ratio of stresses between the confined amorphous phase and the crystalline lamellae evolves due to the fragmentation of the crystalline lamellae as well as the fibrillation and recrystallization processes. Thus, the coupling slowly tends towards a series model. From these considerations, Deplancke et al. [55] recently developed a scalar rheological model (corresponding to a pure elongation one-dimensional model) based on the formulation proposed by Humbert et al. [54] for the intermolecular chain forces within the crystalline structure. Evolving

mechanical coupling between crystalline lamellae and confined amorphous phase occurring during the plastic deformation of the crystalline structure was introduced. Thus, their model is able to fairly describe the deformation mechanisms of semi-crystalline polymers with high molecular weight.

To use this model at a larger scale, such as polymer-process modelling and simulations, a three-dimensional formulation is needed. Thus, the aim of this paper is to propose, from this scalar model, physical, mechanical and implementable three-dimensional constitutive equations for Ultra High Molecular Weight PolyEthylene (UHMWPE) behavior. Thus, the model has to account for the evolution of the mechanical coupling between crystalline lamellae and confined amorphous phase, i.e. fibrillation process occurring during the deformation process of the material. In section 2, the analog form of the scalar model basis is recalled and its transformation into a three-dimensional model is explained. In section 3, a three-dimensional formulation is proposed according to the philosophy of the scalar model. The main challenge remains the 3D modelling of the intermolecular resistance within the crystalline structure. Section 4 is dedicated to the model validation from experimental quasi-static tests and dynamic loading tests.

## 2. Scalar constitutive model

To simulate the true stress-true strain behavior of UHMWPE over a wide range of strain rates and temperatures, Deplancke et al. [55] have developed a scalar rheological model based on an evolving mechanical coupling between the confined amorphous phase and the crystalline lamellae. Analog representation of their model is presented in Figure 3. The model consists in two networks, "intermolecular resistance network" and "molecular network resistance", acting in parallel as shown in Figure 3. The “intermolecular resistance”, corresponding to the upper branch, comes from the connections (density of physical nodes) between crystalline lamellae and confined amorphous phase within the structure. In the latter, this network will be called “crystal network” and will be denoted ‘CN’. It characterizes the deformation of crystalline lamellae and the confined amorphous phase. During the polymer deformation, chains which are pulled out from the crystalline lamellae and the confined amorphous phase tends towards a fibrillar structure. Thus, as discussed above, we need to implement a strain-dependent evolving mechanical coupling between crystalline lamellae and confined amorphous phase into the crystal network. This is schematically displayed in Figure 3, by a diagonal line meaning that, initially the two branches are neither in parallel nor in series but in an intermediate state. During the plastic deformation, fibrillation process occurs leading to a fundamental change of the polymer microstructure. During that phase the mechanical coupling evolve from neither parallel nor series configuration towards a series configuration. On the other hand, the lower branch depicts the molecular arrangement of the macromolecular network (MN). Each structure (crystalline lamellae, confined amorphous phase and macromolecules) has its own mechanical behavior. Thus, crystalline lamellae exhibit elastic-viscoplastic behavior. Confined

amorphous phase behave as hyperelastic-viscoplastic material. As for the macromolecular network, its behavior is hyperelastic with an important viscous component due to the reptation of the polymer chains.

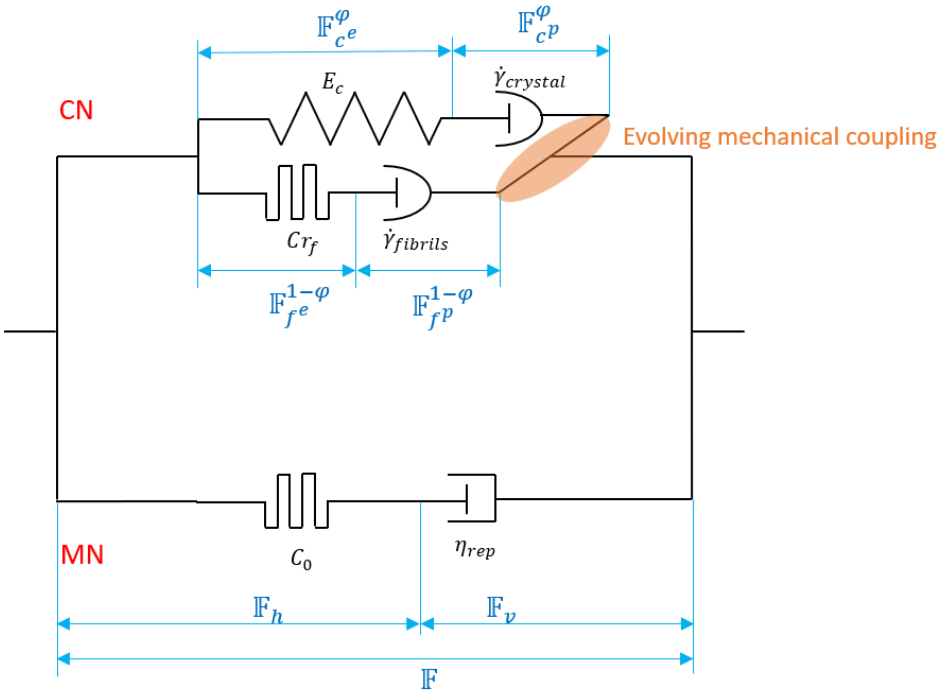


*Figure 3: Mechanical analog representation of the proposed three-dimensional constitutive model adapted from Deplancke et al. [55] for predicting the thermomechanical behavior of UHMWPE. (CN: intra-chain cohesive forces in the crystal network, MN: macromolecular network).*

According to the scalar model developed by Deplancke et al. [55] and the formalism described by the analog representation (see Figure 3), the main scalar relationships describing the UHMWPE mechanical behavior are summarized in eq. (1) for strain $\varepsilon$ and eq. (2) for stress $\sigma$:

$$\varepsilon_{total} = \varepsilon_{CN} = \varepsilon_{MN}$$
$$\text{with } \varepsilon_{CN} = (1-\varphi)\left(\varepsilon_{f^e} + \varepsilon_{f^p}\right) + \varphi(\varepsilon_{c^e} + \varepsilon_{c^p}) \tag{1}$$

$$\sigma_{total} = \sigma_{CN} + \sigma_{MN}$$
$$\text{with } \begin{cases} \sigma_{CN} = (1-\varphi)\sigma_f + \varphi\sigma_c \\ \sigma_c = k\sigma_f \end{cases} \tag{2}$$

where $\varphi$ is the crystal ratio and $k$ is the coupling parameter describing the crystal transformation into fibrils occurring during the deformation of the crystalline structure. The expression (1) can also be found in the work of Bartsczak [9] where it represent the evolution of the residual true stress during the material deformation of semi-crystalline polymers. The subscripts *'CN'* and *'MN'* refer to the 'intra

chain cohesive forces in the crystal network' and 'macromolecular network' branches, respectively. Subscripts *'c'* and *'f'* are related to crystalline lamellae and confined amorphous phase/fibrils respectively whereas *'e'* and *'p'* define the elastic and the plastic deformations, respectively.

As shown by eq. (2), the mechanical coupling is expressed as a proportional relationship between crystal $\sigma_c$ and fibril $\sigma_f$ stresses through parameter $k$. Its evolution, defined by a phenomenological relationship by Deplancke et al. [55], is a function of the plastic deformation of the crystalline lamellae $\varepsilon_{pl}$:

$$k = (k_{init})^{1-\frac{\varepsilon_{pl}}{\varepsilon_{nat}}} \tag{3}$$

where $k_{init}$ is the initial value for the mechanical coupling fitted on the elastic modulus for a large range of polyethylene and $\varepsilon_{nat}$ corresponds to the deformation for which the fibrillar state is reached. When there is no plastic deformation, $k$ is equal to $k_{init}$. It corresponds to the initial microstructural state of the material. In the contrary, when $\varepsilon_{pl} = \varepsilon_{nat}$, $k = 1$ which corresponds to the fibrillar state of the material. This arbitrary decreasing function maps the evolution of microstructure from crystal network to a fibrillar state. More details about this function can be found in [55]. The existence of a stress relationship to describe the mechanical behavior leads to the implicit existence of a strain relationship for the evolving mechanical coupling.

Thus, as shown by Figure 3, eqs. (1) and (2), the complexity of the model mainly comes from the strain dependent mechanical coupling between crystalline lamellae and confined amorphous phase of the CN branch. Moreover, for the CN branch and from a numerical point of view, the strain relationship (eq. (1)) is described by series configuration while the stress relationship (eq. (2)) is described by parallel configuration. The difference between these two configurations should be considered while developing three-dimensional constitutive equations according to the deformation mechanisms introduced by Deplancke et al. [55].

## 3. Three-dimensional constitutive model

The three-dimensional constitutive model is developed in agreement with the formalism established by the analog representation (Figure 3) and the scalar model developed by Deplancke et al. [55]. According to this, the total stress tensor $\mathbb{T}$ is given by the sum of the crystal network stress tensor $\mathbb{T}_{CN}$ (combination of Cauchy stress tensor and hyperelastic stress tensor) and the macromolecular stress tensor $\mathbb{T}_{MN}$ (hyperelastic and viscous contributions):

$$\mathbb{T} = \mathbb{T}_{CN} + \mathbb{T}_{MN}. \tag{4}$$

Moreover, these two networks acting in parallel imply that their deformation gradients, denoted $\mathbb{F}_{CN}$ for the crystal network and $\mathbb{F}_{MN}$ for the macromolecular network, are equals to the total deformation gradient tensor $\mathbb{F}$ such as:

$$\mathbb{F} = \mathbb{F}_{CN} = \mathbb{F}_{MN}. \tag{5}$$

The finite deformation kinetics presented in Figure 4 makes reference to the various configurations (initial, intermediate and current or final). The significance of the different deformation gradient will be explained in the following.

In the present work, we propose to extend the scalar physical model developed by Deplancke et al. [55] into a three-dimensional thermomechanical physical and implementable model. The main challenge is to propose a 3D description able to represent the phenomena involve in the crystal deformation and the mechanical coupling evolving from crystalline structure (crystalline lamellae and confined amorphous phase) towards fibrillar structure [56].

### 3.1. Preliminary kinetics

The kinematics of the finite strain allows describing the evolution of a solid particle from its reference state to its current state through various configurations. Let us denoted B a deformable body and X the spatial position of the solid particle A within B. The motion of B induces the displacement of the solid particle from X to x. The evolution of the particle position across the different configurations is described by the deformation gradient, such as:

$$\mathbb{F} = \frac{\partial \mathrm{x}}{\partial \mathrm{X}}. \tag{6}$$

Using the polar decomposition, the stretches and rotations contributions can be decomposed from the deformation gradient as follows:

$$\mathbb{F} = \mathbb{R}\mathbb{U} = \mathbb{V}\mathbb{R} \tag{7}$$

where $\mathbb{R}$ is the pure rotation tensor and $\mathbb{U}$ and $\mathbb{V}$ are the pure right and left stretch tensor, respectively. This decomposition can be performed on every deformation gradient encounter in this study. The velocity gradient, representing the deformation rate, is defined from the time derivative of $\mathbb{F}$ by:

$$\mathbb{L} = \dot{\mathbb{F}}\mathbb{F}^{-1}. \tag{8}$$

As a standard, it exists a unique additive decomposition for the velocity gradient $\mathbb{L}$ such as:

$$\mathbb{L} = \mathbb{D} + \mathbb{W} \tag{9}$$

where the symmetric tensor $\mathbb{D}$ is the rate of deformation tensor and the skew-symmetric tensor $\mathbb{W}$ is the spin tensor.

### 3.2. Intra-chain cohesive forces in the crystal network

In the analog representation (see Figure 3), the deformation balance between crystal and confined amorphous phase within the crystalline structure is neither described by a parallel model nor a series model. The coupling between these two quantities evolves during the deformation process and slowly converges towards a series model when $k = 1$. It implies that the deformation rates of the crystalline lamellae and the confined amorphous phase are different but linked together.

In order to the represent this coupling, the developed constitutive equations should consider the quasi-parallel to series model evolution from the deformation gradient. According to the analog representation (see Figure 3), the crystal network can be divided into two phases: crystalline lamellae and confined amorphous phase which aim to become fibrils. Moreover, each phase is represented, on the analog representation, by a spring in series with a viscous dashpot describing the initial stiffness and the viscoplastic behavior of the material respectively. Detailed representation of the crystal network finite deformation kinetics is represented in Figure 4. One dashpot is related to the fragmentation of the crystalline lamellae while the other dashpot is related to the sliding of fibrils against each other.

Let $\varphi$ be the crystal ratio of the polymer. Let us denote by the subscripts '*f*' and 'c', the tensors related to the confined amorphous phase/fibrils and crystalline lamellae respectively. We propose to multiplicatively decompose the deformation gradient of the crystal network into confined amorphous phase/fibril and crystalline parts to take into account the material microstructure and its evolution during the deformation. Thus, to have an analog representation to the rheological model proposed by Deplancke et al. [55], we propose to raise $\mathbb{F}$ to the power with respect to the crystal ratio:

$$\mathbb{F}_{CN} = \mathbb{F}_f^{1-\varphi}\mathbb{F}_c^{\varphi} \tag{10}$$

with

$$\begin{cases} \mathbb{F}_f = \mathbb{F}_{f^e}\mathbb{F}_{f^p} \\ \mathbb{F}_c = \mathbb{F}_{c^e}\mathbb{F}_{c^p} \end{cases} \tag{11}$$

$\mathbb{F}_{c^p}^{\varphi}$ refers to the crystalline lamellae viscoplastic deformation from the initial configuration $\Omega_0$ to the first intermediate configuration $\Omega_{int1}^{cn}$. $\mathbb{F}_{c^e}^{\varphi}$ refers to the elastic deformation from the first intermediate configuration to the second intermediate configuration $\Omega_{int2}^{cn}$. $\mathbb{F}_{f^p}^{1-\varphi}$ refers to the confined amorphous phase/fibrils viscoplastic deformation from the second intermediate configuration to the third intermediate configuration $\Omega_{int3}^{cn}$. Finally, $\mathbb{F}_{f^e}^{1-\varphi}$ refers to the confined

amorphous phase/fibrils viscoelastic deformation from the third intermediate configuration to the current configuration $\Omega_1$.

Demonstration of the relationship (10), valid only at small strains or for small step time, is available in Appendix A.

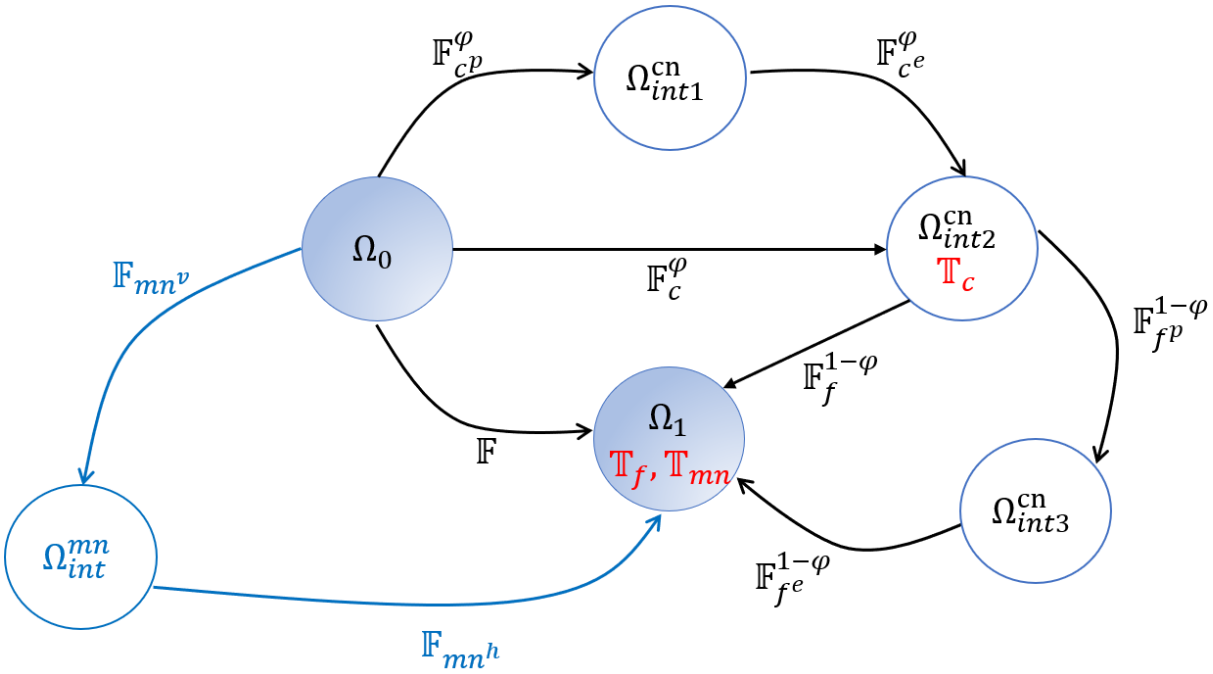


*Figure 4: Finite deformation kinetics. The total deformation gradient $\mathbb{F}$ maps the deformation between the initial configuration $\Omega_0$ and the current configuration $\Omega_1$ through various intermediate configurations $\Omega_{int}$. The decomposition procedure applied to each network is represented in accordance with the crystal ratio and the elastic/viscous-plastic deformation associated to each phase. Each intermediate configuration corresponds to a deformation state of the material. Stresses in the elastic configurations are firstly calculated following by the plastic deformation behavior. The total stress is calculated in the current configuration $\Omega_1$* by rotation of the stress tensor $\mathbb{T}_c$.

Unlike the scalar model (see eq. (2)), we propose to represent the mechanical coupling between crystalline lamellae and confined amorphous phase through a relationship linking the deformation gradients of the crystal and confined amorphous phase/fibrils components. This solution aims to reduce the computation time of the modelling. However, indirect relationship, linked to the non-linearity of the stress tensors, exists between the two mechanical couplings (depending on stress and depending on strain). Thus, we assume the following relationship

$$\mathbb{F}_c = \left(\mathbb{F}_f\right)^{\zeta} \tag{12}$$

where the parameter $\zeta$ represents the mechanical coupling from deformation gradient viewpoint. Parallel model is obtained when $\zeta_{parallel} = 1$, while the series corresponds to $\zeta_{series} = \frac{E_f}{E_c} J_f^{\zeta-1}$ (where $J_f = \det \mathbb{F}_f$). Demonstration of this relationship at small strains is available in Appendix B.

### 3.2.1. Crystalline lamellae

The elastic behavior of the crystalline lamellae is described by the Cauchy stress tensor, $\mathbb{T}_c$, which considers the high rigidity of the crystal network through the fourth order stiffness tensor $\mathbb{C}^e$, such as

$$\mathbb{T}_c = \frac{1}{J_{c^e}} \mathbb{C}_{c^e} \ln \mathbb{V}_{c^e} \tag{13}$$

where $J_{c^e} = \det \mathbb{F}_{c^e}$ is the volume change, $\ln \mathbb{V}_{c^e}$ is the Hencky strain measure with $\mathbb{F}_{c^e} = \mathbb{V}_{c^e} \mathbb{R}_{c^e}$. Assuming the material is elastic linear, the stiffness tensor considers only two independent parameters, the elastic modulus $E_c$ and the Poisson's ratio $\nu_c$of the crystalline lamellae.

The end of the elastic regime of the crystalline lamellae is defined by the yield strength corresponding to the dashpot element $\dot{\gamma}_{crystal}$ in the rheological model (see Figure 3). It is generally admitted in the literature [14–17,57,58] that the yield behavior is due to the influence of thermally activated process(es). One of the first theories developed for the prediction of the yield stress of polymers was proposed by Eyring [14]. This theory is based on the jump of molecules from one equilibrium position to another when they overcome the activation energy barrier. According to the Eyring model [14], the flow rule is expressed as:

$$\dot{\gamma}_{c^p} = \frac{k_B T}{h} e^{-\Delta H_c / k_B T} \sinh\left(\frac{V_c \tau_c}{k_B T}\right) \tag{14}$$

with 'c' subscript referring to values associated to the crystalline lamellae and where $\dot{\gamma}_{c^p}$ is the shear plastic rate, $k_B$ is the Bolzmann constant, $h$ is the Plank constant, $T$ is the absolute temperature , $\Delta H$ is the activation energy of the secondary relaxation, $V$ is the shear activation volume and $\tau$ is the effective equivalent shear stress defined by:

$$\tau_c = \left[\frac{1}{2} \mathbb{T}'_c : \mathbb{T}'_c\right]^{1/2} \tag{15}$$

with $\mathbb{T}'_c$ the deviatoric part of the Cauchy stress tensor developed in eq. (13).

According to Peterlin [4], the plastic deformation of semi-crystalline polymers occurs in three stages. The first one concerns the plastic deformation of the spherulites. The second one is due to the micro-necking occurring during the plastic deformation which induces an evolution of the spherulites into fibrils within the crystalline structure. The third stage of deformation is due to the plastic deformation of the fibrils.

To characterize the second stage of plastic deformation, Deplancke et al. [55] have developed an evolving relationship to describe the mechanical coupling between spherulites and confined amorphous phase leading to fibrillar structure. Using a phenomenological relationship given by eq. (3), they expressed the coupling parameter as a function of the plastic deformation of the crystalline

lamellae. Considering the shift of the mechanical coupling from the stress towards the strain, we choose to slightly modify the expression given by Deplancke et al. [55]:

$$\zeta = \left(\zeta_{init} - \zeta_f\right) \exp\left(-\frac{\gamma_{c^p}}{\gamma_{nat}}\right) + \zeta_f \tag{16}$$

where $\gamma_{c^p}$ is the plastic shear of the crystalline lamellae deduced from eq. (14), $\gamma_{nat}$ designates the deformation for which the fibrillar state is reached, $\zeta_{init}$ characterizes the initial mechanical coupling between the crystalline lamellae and the confined amorphous phase and $\zeta_f$is the final value of the mechanical coupling equal to the ratio of elastic modulus between the confined amorphous phase and the crystalline lamellae. The $\zeta$ parameter decreases from 1 (parallel model) to the ratio of stiffness $E_f/E_c$ (series model). It corresponds to a reality of the deformation mechanisms (fibrillation process) of high-molecular weight semi-crystalline polymers and leading to an evolution of microstructure.

The plastic deformation of the material is supposed to be an isochoric transformation. Thus, using eqs. (9), (13) and (15), the plastic rate of deformation tensor of the crystalline lamellae $\mathbb{D}_{c^p}$ is defined by:

$$\mathbb{D}_{c^p} = \frac{\dot{\gamma}_{c^p}}{\sqrt{2}\tau_c}\mathbb{T}'_c \tag{17}$$

where $\sqrt{2}\tau_c$is the norm of $\mathbb{T}'_c$ and $\dot{\gamma}_{c^p}$ matches with the magnitude of $\mathbb{D}_c^p$.

### 3.2.2. Confined amorphous phase

To represent the important elongation and the locking of the confined amorphous phase within the crystal network, the 8-chain model developed by Arruda and Boyce [21] is used. This hyperelastic model is based on deformation-difference description of the strain measure and on non-linear elasticity (Langevin spring). Two independent parameters, the rigidity modulus of the confined amorphous phase $E_f$ and the number of rigid links between entanglements $N_f$, are needed to describe the confined amorphous phase deformation behavior. The principal components of the stress tensor $\mathbb{T}_f$ are defined by:

$$\mathbb{T}_{f\,i} = E_f \frac{\sqrt{N_f}}{3}\mathcal{L}^{-1}\left(\frac{\lambda_{chain}}{\sqrt{N_f}}\right)\frac{\lambda_i^2 - \lambda_{chain}^2}{\lambda_{chain}}, \quad i = 1,2,3 \tag{18}$$

where $\mathcal{L}^{-1}$ is the inverse of the Langevin function, $\lambda_i$ are the principal component of the elastic stretch tensor of the confined amorphous phase $\mathbb{V}_{f^e}$ and $\lambda_{chain} = \sqrt{(\lambda_1^2 + \lambda_2^2 + \lambda_3^2)/3}$ is the elastic stretch of each chain segment.

Under the applied loading, the confined amorphous phase will reach their maximum elastic deformation. Thus, at large deformation, after fibrillation process, plastic deformation of the fibrils

will occur. In the analog representation (see Figure 3), this plasticity is illustrated by the dashpot noted "$\mu_{fibrils}$" in series with the non-linear Langevin spring. As previously, the Eyring model [14] is used to simulate the flow rule of the fibrils:

$$\dot{\gamma}_{f^p} = \frac{k_B T}{h} e^{-\Delta H_f / k_B T} \sinh\left(\frac{V_f \tau_f}{k_B T}\right), \tag{19}$$

with '$f$' subscript referring to fibrils and where all the parameters have the same significance as eq. (14). Thus, $\dot{\gamma}_{f^p}$ is the plastic shear rate associated to fibrils and $\tau_f$ is the effective equivalent stress related to the fibrils defined as:

$$\tau_f = \left[\frac{1}{2}\mathbb{T}'_f : \mathbb{T}'_f\right]^{1/2} \tag{20}$$

with $\mathbb{T}'_f$ the deviatoric part of the stress tensor constructed from the 8-chain model and developed in eq. (18).

The plastic transformation related to fibrils is also assumed to be isochoric. Thus, the rate of deformation tensor related to fibrils $\mathbb{D}_{f^p}$ is expressed as:

$$\mathbb{D}_{f^p} = \frac{\dot{\gamma}_{f^p}}{\sqrt{2}\tau_f} \mathbb{T}'_f \tag{21}$$

where $\sqrt{2}\tau_f$ is the norm of $\mathbb{T}'_f$ and $\dot{\gamma}_{f^p}$ matches with the magnitude of $\mathbb{D}_{f^p}$.

#### 3.2.3. Crystalline network

The stress tensor in the crystalline network is obtained from the summation of the stress contributions of the crystalline lamellae and the confined amorphous phase/fibrils (eqs. (13) and (18)). By introducing $\mathbb{T}_c$ in the same configuration than $\mathbb{T}_f$, the stress tensor in the crystalline network $\mathbb{T}_{CN}$ is given by:

$$\mathbb{T}_{CN} = (1-\varphi)\mathbb{T}_f + \varphi \mathbb{R}_f^{1-\varphi} \mathbb{T}_c \mathbb{R}_f^{(1-\varphi)^T} \tag{22}$$

where $\mathbb{R}_f$ is the pure rotation tensor of the confined amorphous phase, deduced from eq. (7).

### 3.3. Macromolecular network

The macromolecular network describes the molecular resistance of the material to the orientation of the polymer chain segments [41]. The plastic deformation of the material allows more flexibility of the polymer chain segments highlighted by relaxation mechanisms and molecular reorganization of the material. The polymer chain segments tend to align in the loading direction leading to important stress increase. These behaviors are characterized in the Figure 4 by a non-linear spring acting in series with

a viscous dashpot. The non-linear spring corresponds to the stretching of the network in respect of the temperature of the material. The dashpot illustrates the molecular relaxation of the polymer chain segments through their reptation mechanisms.

Thus, the deformation gradient $\mathbb{F}_{MN}$ can be decomposed into a hardening component $\mathbb{F}_{mn^h}$, describing the stretching of the material, and a viscous component $\mathbb{F}_{mn^v}$ describing its molecular relaxation, such as:

$$\mathbb{F}_{MN} = \mathbb{F}_{mn^h}\mathbb{F}_{mn^v} \tag{23}$$

where $\mathbb{F}_{mn^v}$ is defined from the initial configuration $\Omega_0$ to the intermediate configuration $\Omega_{int}^{mn}$ associated to the macromolecular network and $\mathbb{F}_{mn^h}$ is defined from the intermediate configuration $\Omega_{int}^{mn}$ to the current configuration $\Omega_1$.

The stretching of the macromolecular network leads to a strong molecular chain orientation and locking phenomenon of the macromolecular chains. Among the hyperelastic models available in the literature, only few of them [21–23,59,24] are able to reproduce such a phenomenon. One of them is the 8-chain model [21] developed by Arruda and Boyce and already introduced previously:

$$\mathbb{T}_{mn_i} = C_m \frac{\sqrt{N_m}}{3\lambda_{chain}} \mathcal{L}^{-1}\left(\frac{\lambda_{chain}}{\sqrt{N_m}}\right)\left(\lambda_i^2 - \lambda_{chain}^2\right), \quad i = 1,2,3 \tag{24}$$

where $\mathcal{L}^{-1}$ is the inverse of the Langevin function, $\lambda_i$ are the principal component of the macromolecular hardening stretch tensor $\mathbb{V}_{mn^v}$. $C_m$ is the hardening modulus of the 8-chain model, $N_m$ is the number of rigid links between entanglements.

To define the probability of the chain disentanglement during the deformation process, a viscous dashpot was added in series to the non-linear spring. It described the possible reptation of the polymer chain which occurs at large deformation. According to the works of de Gennes [60], Doi and Edwards [61], the dynamic viscosity $\eta_{rep}$ can be expressed as:

$$\eta_{rep} = G_{rep}M^3 \tag{25}$$

where $G_{rep}$ is a parameter describing the proportionality between the viscosity and the molecular mass $M$. Thus, the rate of plastic deformation induced by the reptation of the macromolecular chain $\mathbb{D}_{rep}$ is expressed by:

$$\mathbb{D}_{rep} = \frac{\mathbb{T}'_{mn}}{\eta_{rep}}. \tag{26}$$

## 4. Model validation

This model has been specially developed to predict the mechanical behavior of Ultra High Molecular Weight Semi-crystalline polymers. The validation of the model focuses on the UHMWPE at

10.5 Mg.mol$^{-1}$ investigated by Deplancke et al. [55]. The parameters used for the model validation are detailed in Table 1. The same set of parameters is used for all the simulations.

*Table 1: Material properties and model parameters used for the numerical predictions of the mechanical behavior of UHMWPE with a molecular weight of 10.5 Mg.mol$^{-1}$.*

| **Intermolecular resistance within the crystalline structure** | | |
|---|---|---|
| **Crystalline Lamellae** | | |
| • Elastic modulus | $E_c$ **(GPa)** | 27 |
| • Poisson's ratio | $\nu_c$ | 0.3 |
| • Activation volume | $V_c$ **(m$^3$)** | 2.15x10$^{-27}$ |
| • Activation energy | $\Delta H_c$ **(J)** | 1.98x10$^{-19}$ |
| **Confined amorphous phase** | | |
| • Elastic modulus | $E_f$ **(MPa)** | 2.6 |
| • Number of rigid links between entanglement | $N_f$ | 1.02 |
| • Activation volume | $V_f$ **(m$^3$)** | 4.05x10$^{-27}$ |
| • Activation energy | $\Delta H_f$ **(J)** | 1.98x10$^{-19}$ |
| **Mechanical coupling** | | |
| • Initial mechanical coupling between crystalline lamellae and confined amorphous state | $\zeta_{init}$ | 0.05 |
| • Deformation for which the fibrillar state is reached | $\gamma_{nat}$ | 0.8 |

| **Macromolecular network** | | |
|---|---|---|
| • Rubber modulus | $C_m$ **(MPa)** | 2.1 |
| • Number of rigid links between entanglement | $N_m$ | 1.05 |
| • Activation volume | $V_m$ **(m$^3$)** | 1.029x10$^{-25}$ |
| • Activation energy | $\Delta H_m$ **(J)** | 9.29x10$^{-20}$ |
| • Proportional parameter between the viscosity and molecular weight | $G_{rep}$ **(MPa mol$^3$ kg$^{-3}$ s$^{-1}$)** | 1.05 |

Compressive tests performed at room temperature and at different strain rates were used to validate the model. A good agreement is observed in Figure 5 between experimental results (dot) and numerical predictions (solid line) over 6 decades of strain rates for both the loading and unloading parts. At 20% strain and 10 s$^{-1}$, the mechanical behavior of UHMWPE is slightly overestimated due to the presence of non-negligible self-heating, not yet considered at this stage.

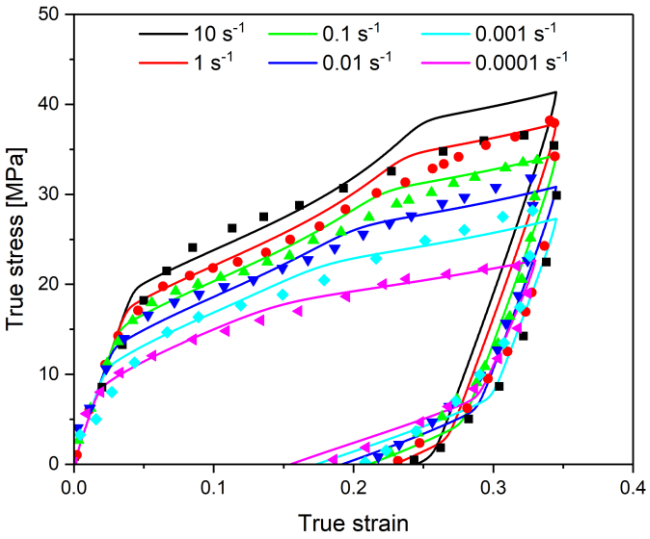


*Figure 5: Comparison between experimental results (dot) from Deplancke et al. [55] and numerical predictions (solid line) in the case of compressive loading performed at different strain rates.*

As mentioned in the section 3, to describe the mechanical behavior of Ultra High Molecular Weight semi-crystalline polymers, three contributions are needed: crystalline lamellae, confined amorphous phase and macromolecular network. Figure 6 presents the mechanical behavior associated to each of these contributions. Thus, at small strain, the mechanical behavior of the polymer is mainly due to the crystalline lamellae. During this stage, dislocation of the crystalline lamellae is observed, leading to the fibrillation process. Thus, when the yield point is reached, the mechanical behavior of the polymer is mainly due to the stretching of the confined amorphous phase in the loading direction. From a morphological point of view, the different crystal sizes spread in the polymer will act as entanglement nodes of the amorphous chains. Thus, when the smallest chains are fully stretched between the entanglement nodes, a third mechanism is highlighted. It consists in the reptation of the chains and the stretching of the longest amorphous chains until locking of the polymer chains. When we unload the material, the first contribution to appear is the one due to the crystalline lamellae branch which describe the elastic linear recovery of the material. From a physical point of view, this recovery comes from the instant release of the stored elastic energy of the crystalline blocks (reticulation nodes) and the stretched confined amorphous phase. When the crystalline lamellae branch finish unloading, the unloading of the confined amorphous phase branch is more visible and contribute to the short-term viscoelastic recovery of the polymer.

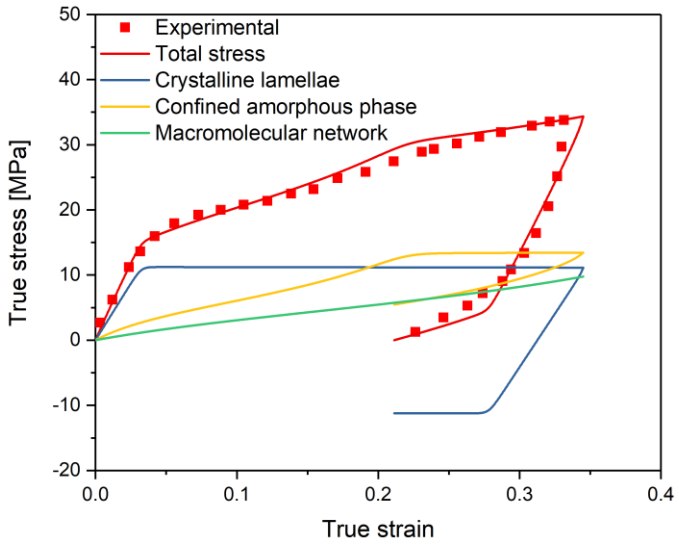


*Figure 6: Contribution of the macromolecular network, crystalline lamellae and confined amorphous phase in the deformation mechanisms of Ultra High Molecular Weight semi-crystalline polymers. Investigation on compression loading performed at room temperature and 0.1 $s^{-1}$ (Experimental results from Deplancke et al. [55]).*

We also investigate the large strain behavior of UHMWPE submitted to compressive loading at room temperature and several strain rates. Numerical predictions are presented in Figure 7. We can observe, at large strain, an important contribution of the macromolecular network leading to the locking of the polymer chains.

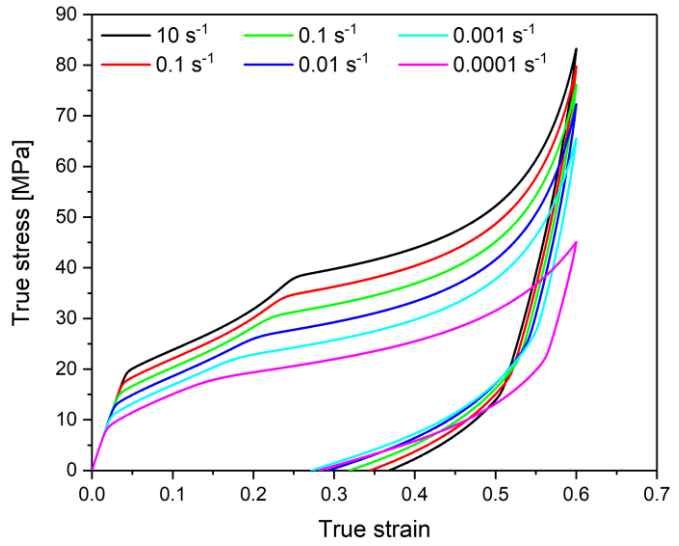


*Figure 7: Numerical predictions of the large strain behavior of UHMWPE submitted to compressive loading at room temperature for different strain rates.*

Cycling behavior of UHMWPE at 298 K and 0.001 $s^{-1}$ is investigated and numerical predictions are presented on Figure 8. For several cycles, the energy dissipation seems quite identical. Thus, submitted to cycling loading, UHMWPE keeps almost all its good mechanical properties.

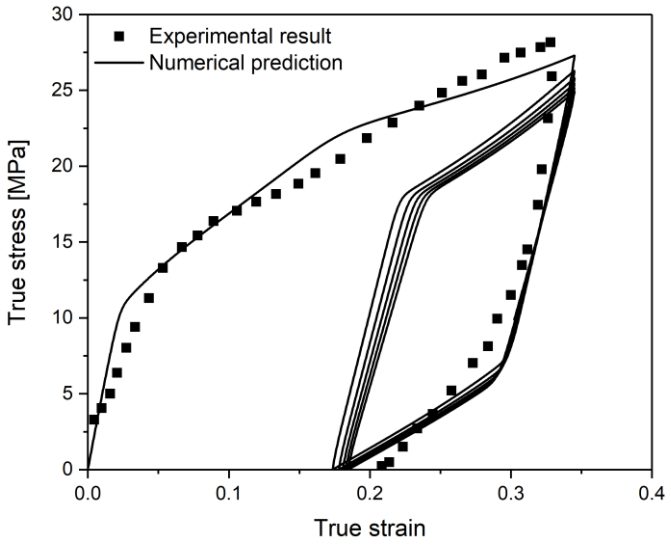


*Figure 8: Investigation of the mechanical behavior of UHMWPE during compressive cycling loading. Numerical predictions obtained for a test performed at 298 K and 0.001 $s^{-1}$. (Experimental results from Deplancke et al. [55])*

## 5. Conclusion

Ultra-High Molecular Weight PolyEthylene exhibits deformation mechanisms quite different from usual semi-crystalline polymers one because of their very long macromolecular chains, which prevent chain disentanglement even at temperature well above the melting point. Deplancke et al. [55] developed a scalar numerical model based on the evolution of the mechanical coupling between crystalline lamellae and confined amorphous phase during the deformation: it is taken into account through a stress relationship. In the present paper, we propose a route to implement such a rheological model in a three-dimensional mechanical modelling.

Indeed, we have developed a three-dimensional model to predict the mechanical behavior of UHMWPE while taking into account the evolution of microstructure, between crystalline lamellae and confined amorphous phase, during the deformation process. Unlike the scalar model, the mechanical coupling of the three-dimensional model has been introduced as a relationship on the deformation gradient. Even though the scalar and the three-dimensional model show non-negligible differences, both share the same philosophy regarding the deformation mechanisms of UHMWPE. Three main relationships govern the deformation behavior of the material: (i) a multiplicative decomposition of the deformation gradient with respect of the crystal ratio, (ii) a relationship which describe the repartition of deformation between crystalline lamellae and confined amorphous phase and (iii) an evolution of the repartition of deformation between crystalline lamellae and confined amorphous phase during the plastic deformation of the crystalline deformation.

The results of this study focus on the strain rate dependence of UHMWPE submitted to compressive loadings. The numerical predictions show a fairly good agreement with the experimental results for both loading and unloading behavior. At large deformation, the numerical prediction clearly exhibits three distinct behaviors. At small strain, the deformation is mainly due to the crystalline lamellae.

When the yield point is reached, fragmentation of the crystalline lamellae and stretching of the confined amorphous phase leads to the fibrillation of the crystal network. Thus, for intermediate strains, ranged from the yield point to the orientational hardening, the polymer behavior is governed by the behavior of the fibrils. Then, at large deformation, when the fibrils reached their maximum stretching between reticulation nodes (assumed to be small crystals), disentanglement of the amorphous chains will take place leading to the orientational hardening of the material. Based on well-known deformation mechanisms involved in semi-crystalline polymers, this model remains realistic and reliable even beyond the range of experimental data on which the model parameters have been adjusted.

Only the strain rate dependence of the material is investigated in this work. As polymers are also strongly sensitive to the temperature, it is necessary to identify properly the model parameters not only in function of the strain rate, but also in function of the temperature. In addition, it will be interesting to investigate different configurations such as tensile and shear loadings while accounting for the true kinematics of the deformable solid [62].

However, because the three-dimensional model shows good agreement with the experimental results, it could be interesting to implement it in a finite element software to simulate various applications such as polymer coating by cold-spray [63] or hydrodynamic cavitation erosion [64] which correspond to the initial applications motivating the development of the rheological model.

## Appendix A: Demonstration of eq. (9) regarding the multiplicative decomposition of the deformation gradient

In this paper, we introduced a new formulation for the multiplicative decomposition of the deformation gradient for semi-crystalline polymers with respect to the crystalline ratio:

$$\mathbb{F} = \mathbb{F}_f^{1-\varphi}\mathbb{F}_c^{\varphi} \tag{A.1}$$

By assuming that the deformation gradient increment is small ($\Delta\mathbb{F} \ll \mathbb{I}$), we can perform a first order development of the deformation gradients such as:

$$\begin{cases} \mathbb{F}_f^{1-\varphi} \cong \mathbb{I} + (1-\varphi)\Delta\mathbb{F}_f \\ \mathbb{F}_c^{\varphi} \cong \mathbb{I} + \varphi\Delta\mathbb{F}_c \end{cases}. \tag{A.2}$$

Thus, in the case of infinitesimal strain, the total deformation tensor $\varepsilon$ is written:

$$\varepsilon = \mathbb{F}\mathbb{F}^T - \mathbb{I} \cong \left[\left(\mathbb{I} + (1-\varphi)\Delta\mathbb{F}_f\right).\left(\mathbb{I} + \varphi\Delta\mathbb{F}_c\right)\right].\left[\left(\mathbb{I} + \varphi\Delta\mathbb{F}_c^T\right).\left(\mathbb{I} + (1-\varphi)\Delta\mathbb{F}_f^T\right)\right] - \mathbb{I}. \tag{A.3}$$

By developing eq. (A.3) and keeping only the first order, we obtain:

$$\varepsilon = \Delta\mathbb{F}_f + \Delta\mathbb{F}_{\mathrm{f}}^{\mathrm{T}} + \varphi\left(\Delta\mathbb{F}_c + \Delta\mathbb{F}_c^{\mathrm{T}} + \Delta\mathbb{F}_f + \Delta\mathbb{F}_{\mathrm{f}}^{\mathrm{T}}\right) + O(\Delta\mathbb{F}_i\Delta\mathbb{F}_j). \tag{A.4}$$

where $O(\Delta\mathbb{F}_i\Delta\mathbb{F}_j)$ corresponds to the residual of the development of order 2 and above.

In analogy with the rheological model, law of mixture can be used as a first approximation. Thus, the total deformation tensor can also be view as the summation of the deformation tensor of each branch as a first approximation. Thus, the square of the total deformation tensor can be expressed as:

$$\varepsilon = (1-\varphi)\mathbb{V}_f^2 + \varphi\mathbb{V}_c^2 \tag{A.5}$$

At small strain or small deformation increment, we can assume that the increment of the deformation tensor is negligible. Thus, the deformation tensor of each branch is assumed to be equal to the deformation gradient given at the first order by:

$$\begin{cases}\mathbb{F}_f \cong \mathbb{I} + \Delta\mathbb{F}_f \\ \mathbb{F}_c \cong \mathbb{I} + \Delta\mathbb{F}_c\end{cases} \tag{A.6}$$

Knowing that $\mathbb{V}_i^2 = \mathbb{F}_i\mathbb{F}_i^T$ with $i = c, f$, and introducing eq. (A.6) into (A.5), at the first order, we have left:

$$\varepsilon = \Delta\mathbb{F}_f + \Delta\mathbb{F}_f^{\mathrm{T}} + \varphi\left(\Delta\mathbb{F}_c + \Delta\mathbb{F}_c^{\mathrm{T}} + \Delta\mathbb{F}_f + \Delta\mathbb{F}_f^{\mathrm{T}}\right) + O\left(\Delta\mathbb{F}_i\Delta\mathbb{F}_j\right). \tag{A.7}$$

At small strain (or small increment of deformation), eqs. (A.4) and (A.7) are equals which let us assume the validity of our formulation (eq. (A.1)) to describe the repartition of strain for a semi-crystalline polymer and more generally for a two-phase material.

**Appendix B: Demonstration of eq. (12) regarding the introduction of the fibrillation process**

In this paper, we introduced the fibrillation process through a relationship between deformation gradients of the confined amorphous phase and crystalline lamellae, respectively $\mathbb{F}_f$ and $\mathbb{F}_c$. The particularity of this model is its capacity to transfer from semi-parallel model to series model using only one equation:

$$\mathbb{F}_c = \left(\mathbb{F}_f\right)^{\zeta} \tag{B.1}$$

where $\zeta$ describes the fibrillation process.

Under the assumption of small deformations, we can assume that the behavior of the confined amorphous phase and crystalline lamellae is linear elastic (to simplify the demonstration) and the pure rotation tensor is equal to identity tensor. It leads to the deformation gradient equals to the pure deformation tensor ($\mathbb{F} = \mathbb{V}$). Thus, at small deformation, we can assume that both behaviors can be modelled by the Cauchy stress tensors with the appropriate mechanical properties. Thus, we have:

$$\begin{cases} \mathbb{T}_c = \dfrac{1}{J_c}\mathbb{C}_c \ln \mathbb{V}_c \\ \mathbb{T}_f = \dfrac{1}{J_f}\mathbb{C}_f \ln \mathbb{V}_f \end{cases}. \tag{B.2}$$

In the case of the series model, the stress tensors are equals. Thus, $\mathbb{T}_c = \mathbb{T}_f$. According to eq. (B.1), and in the case of isotropic materials ($\mathbb{C}_i \equiv E_i, i = c, f$), this equality becomes:

$$\zeta_{series} = \frac{E_f}{E_c} J_f^{\zeta - 1} \tag{B.3}$$

where $J_f$ tends towards 1 as volume change remain weak. Thus, $\zeta_{series}$ tends towards the ratio between the two rigidities.

In the case of parallel model, the deformation tensors are equals. It results that $\mathbb{F}_c = \mathbb{F}_f$. It leads to:

$$\zeta_{parallel} = 1. \tag{B.4}$$

By combining eq. (B.4) into eqs. (10) and (12) (or (B.1)), we obtain the relationship $\mathbb{F} = \mathbb{F}_f = \mathbb{F}_c$, which corresponds to the definition of a parallel model.

Thus, the proposed formulation for the repartition of strain allows to represent both parallel and series model. Moreover, by taking an initial value of $\zeta$, such as $\zeta_{series} < \zeta < \zeta_{parallel}$, we are able to define a model which is neither parallel nor series and which corresponds to the initial microstructure of semi-crystalline polymers. Thereafter, using eq. (16) with the constitutive equations allows to describe an evolution of the microstructure from crystalline network (crystalline lamellae and confined amorphous phase) towards a fibrillar microstructure. Thus, the rheological model evolves from intermediate state (neither parallel nor series model) towards a series model.

**Acknowledgement**

The authors would like to acknowledge the Japan Society for the Promotion of Science who provide a short-term post-doctoral fellowship PE16764 for this work. This work was partly supported by JSPS KAKENHI Grant-in-Aid for Scientific Research (A) 17H01235.

**References**

1. L. Mandelkern, Polymer Journal **17**, 337 (1985).
2. R. Séguéla, Journal of Polymer Science Part B: Polymer Physics **43**, 1729 (2005).
3. B. Xiong, O. Lame, J. Chenal, C. Rochas, and R. Seguela, Express Polymer Letters **10**, 311 (2016).
4. A. Peterlin, Journal of Materials Science **6**, 490 (1971).
5. A. Peterlin, Colloid and Polymer Science **253**, 809 (1975).
6. A. Peterlin, Polymer Engineering & Science **17**, 183 (1977).
7. B. Xiong, O. Lame, J.-M. Chenal, Y. Men, R. Seguela, and G. Vigier, Polymer **118**, 192 (2017).
8. J. Defebvin, S. Barrau, G. Stoclet, C. Rochas, and J.-M. Lefebvre, Polymer **84**, 148 (2016).
9. Z. Bartczak, Polymer Testing **68**, 261 (2018).
10. F. Wang, L. Liu, P. Xue, and M. Jia, Polymers **9**, 96 (2017).
11. C. Mahieux and K. Reifsnider, Journal of Materials Science **37**, 911 (2002).

12. J. Richeton, G. Schlatter, K. Vecchio, Y. Rémond, and S. Ahzi, Polymer **46**, 8194 (2005).
13. R. B. Dupaix and M. C. Boyce, Polymer **46**, 4827 (2005).
14. H. Eyring, The Journal of Chemical Physics **4**, 283 (1936).
15. C. Bauwens-Crowet, Journal of Materials Science **8**, 968 (1973).
16. A. Argon, Philosophical Magazine **28**, 839 (1973).
17. J. Richeton, S. Ahzi, L. Daridon, and Y. Rémond, Polymer **46**, 6035 (2005).
18. O. Gueguen, J. Richeton, S. Ahzi, and A. Makradi, Acta Materialia **56**, 1650 (2008).
19. C. A. Bernard, J. P. M. Correia, and S. Ahzi, Mechanics of Materials **130**, 20 (2019).
20. L. R. Treloar, H. Hopkins, R. S. Rivlin, and J. Ball, in (The Royal Society, 1976), pp. 301–330.
21. E. M. Arruda and M. C. Boyce, Journal of the Mechanics and Physics of Solids **41**, 389 (1993).
22. P. Wu and E. Van Der Giessen, Journal of the Mechanics and Physics of Solids **41**, 427 (1993).
23. A. Gent, Rubber Chemistry and Technology **69**, 59 (1996).
24. L. Gornet, G. Macrkmann, R. Desmorat, and P. Charrier, Constitutive Models for Rubbers VII 265 (2012).
25. A. Pawlak, A. Galeski, and A. Rozanski, Progress in Polymer Science **39**, 921 (2014).
26. S. Patlazhan and Y. Remond, Journal of Materials Science **47**, 6749 (2012).
27. Séguéla, R., Epoly **7**, (2007).
28. S. Ahzi, A. Makradi, R. V. Gregory, and D. D. Edie, Mechanics of Materials **35**, 1139 (2003).
29. E. M. Arruda, M. C. Boyce, and R. Jayachandran, Mechanics of Materials **19**, 193 (1995).
30. A. Mulliken and M. Boyce, International Journal of Solids and Structures **43**, 1331 (2006).
31. J. Yi, M. Boyce, G. Lee, and E. Balizer, Polymer **47**, 319 (2006).
32. J. Richeton, S. Ahzi, K. S. Vecchio, F. C. Jiang, and A. Makradi, International Journal of Solids and Structures **44**, 7938 (2007).
33. L. Anand, N. M. Ames, V. Srivastava, and S. A. Chester, International Journal of Plasticity **25**, 1474 (2009).
34. C. A. Bernard, J. P. M. Correia, S. Ahzi, and N. Bahlouli, International Journal of Material Forming 1 (2016).
35. J. P. Torres and P. M. Frontini, International Journal of Solids and Structures **85**–**86**, 125 (2016).
36. T. Mori and K. Tanaka, Acta Metallurgica **21**, 571 (1973).
37. Y. Benveniste, Mechanics of Materials **6**, 147 (1987).
38. R. Hill, Journal of the Mechanics and Physics of Solids **13**, 189 (1965).
39. O. Gueguen, S. Ahzi, A. Makradi, and S. Belouettar, Mechanics of Materials **42**, 1 (2010).
40. A. Sedighiamiri, T. B. Van Erp, G. W. M. Peters, L. E. Govaert, and J. A. W. van Dommelen, Journal of Polymer Science Part B: Polymer Physics **48**, 2173 (2010).
41. M. Boyce, S. Socrate, and P. Llana, Polymer **41**, 2183 (2000).
42. S. Nikolov, I. Doghri, O. Pierard, L. Zealouk, and A. Goldberg, Journal of the Mechanics and Physics of Solids **50**, 2275 (2002).
43. A. Makradi, S. Ahzi, R. V. Gregory, and D. D. Edie, International Journal of Plasticity **21**, 741 (2005).
44. A. D. Drozdov and J. deC. Christiansen, International Journal of Solids and Structures **45**, 4274 (2008).
45. G. Ayoub, F. Zaïri, M. Naït-Abdelaziz, and J. M. Gloaguen, International Journal of Plasticity **26**, 329 (2010).
46. Z. Bartczak and A. Galeski, Macromolecular Symposia **294**, 67 (2010).

47. C. M. Popa, R. Fleischhauer, K. Schneider, and M. Kaliske, International Journal of Plasticity **61**, 128 (2014).
48. D. Garcia-Gonzalez, R. Zaera, and A. Arias, International Journal of Plasticity **88**, 27 (2017).
49. J. A. W. van Dommelen, M. Poluektov, A. Sedighiamiri, and L. E. Govaert, Mechanics Research Communications **80**, 4 (2017).
50. G. Ayoub, F. Zaïri, C. Fréderix, J. M. Gloaguen, M. Naït-Abdelaziz, R. Seguela, and J. M. Lefebvre, International Journal of Plasticity **27**, 492 (2011).
51. J. P. Torres, P. M. Frontini, M. Machado, and Z. Major, International Journal of Impact Engineering **98**, 52 (2016).
52. J. A. W. van Dommelen, D. M. Parks, M. C. Boyce, W. A. M. Brekelmans, and F. P. T. Baaijens, Journal of the Mechanics and Physics of Solids **51**, 519 (2003).
53. J. Bergstrom and J. Bischoff, The International Journal of Structural Changes in Solids **2**, 31 (2010).
54. S. Humbert, O. Lame, R. Séguéla, and G. Vigier, Polymer **52**, 4899 (2011).
55. T. Deplancke, M. Fivel, and O. Lame, Mechanics of Materials **137**, (2019).
56. C. A. Bernard, T. Deplancke, O. Lame, K. Ogawa, and J.-Y. Cavaillé, EPJ Web of Conferences **183**, (2018).
57. C. Bauwens-Crowet, J. Bauwens, and G. Homes, Journal of Polymer Science Part B: Polymer Physics **7**, 735 (1969).
58. J. C. Bauwens, Journal of Materials Science **7**, 577 (1972).
59. O. Yeoh, Rubber Chemistry and Technology **66**, 754 (1993).
60. P. G. de Gennes, The Journal of Chemical Physics **55**, 572 (1971).
61. M. Doi and S. Edwards, Journal of the Chemical Society, Faraday Transactions 2: Molecular and Chemical Physics **74**, 1818 (1978).
62. C. A. Bernard, D. George, S. Ahzi, and Y. Remond, Mathematics and Mechanics of Solids (under publication) (2020).
63. K. Ravi, Y. Ichikawa, T. Deplancke, K. Ogawa, O. Lame, and J.-Y. Cavaille, Journal of Thermal Spray Technology **24**, 1015 (2015).
64. T. Deplancke, O. Lame, J.-Y. Cavaille, M. Fivel, M. Riondet, and J.-P. Franc, Wear **328**, 301 (2015).